ARTICLE

Cavity Ringdown Spectroscopy of PH_2 Radical in 465–555 nm

Dong-feng Zhao[†], Cheng-bing Qin, Qun Zhang, Yang Chen[*]

Hefei National Laboratory for Physical Sciences at the Microscale and Department of Chemical Physics, University of Science and Technology of China, Hefei 230026, China

(Dated: Received on June 3, 2010; Accepted on July 16, 2010)

Absorption spectra of jet-cooled PH_2 radicals were recorded in the wavelength range of 465–555 nm using cavity ringdown spectroscopy. The PH_2 radicals were produced in a supersonic jet by pulsed direct current discharge of a mixture of PH_3 and SF_6 in argon. Seven vibronic bands with fine rotational structures have been observed and assigned as 0_0^0, 2_0^n, and 2_1^n (n=1–3) bands of the $\tilde{A}^2A_1$-$\tilde{X}^2B_1$ electronic transition. Rotational assignments and rotational term values for each band were re-identified, and the molecular parameters including rotational constants, centrifugal distortion constants, and spin-rotation interaction constants were also improved with reasonably high precision. In addition, large perturbations observed in each quantum number of total angular momentum of the a axis level of the excited vibronic states were briefly discussed.

Key words: PH_2 radical, DC discharge, Cavity ringdown spectroscopy

I. INTRODUCTION

The absorption spectrum of PH_2 ($\tilde{A}^2A_1$-$\tilde{X}^2B_1$) was first observed in the flash photolysis of phosphine (PH_3) by Ramsay [1]. A long progression of absorption bands was reported and assigned to the bending vibration v_2' from 0 to 10 in the upper state. Guenebaut *et al.* also found the same band system in the emission spectrum obtained from the discharge of PH_3 [2, 3]. The first rotational analysis of the spectrum of PH_2 was carried out for the 0_0^0 band by Dixon *et al.* [4], who derived the geometries of PH_2 for both excited and ground vibronic states. Similar studies were extended to higher vibrational levels of v_2''=2 and 3 by Pascat *et al.* [5, 6] and v_2'=1–8 by Berthou *et al.* [7]. Huie *et al.* measured the radiative lifetimes of the excited state with v_2' from 0 to 5 by monitoring the laser-induced fluorescence (LIF) [8]. The early studies for the rotational and vibrational spectra of PH_2 $\tilde{X}^2B_1$ state were carried out by Davies *et al.* [9, 10] and McKellar *et al.* [11, 12] by means of laser magnetic resonance spectroscopy. Curl *et al.* and Kakimoto *et al.* precisely determined the hyperfine parameters for the $\tilde{A}^2A_1(0^0)$ state using Doppler-limited LIF spectroscopy and intermodulated fluorescence spectroscopy, respectively [13, 14]. In concurrence with these studies, Endo *et al.* observed the microwave spectra of PH_2, and derived the molecular constants for the ground state [15, 16]. Chen *et al.* reported the LIF spectrum of jet-cooled PH_2 with a spectral resolution of ∼0.2 cm^{-1} for the first time [17]. A Doppler-limited laser excitation spectrum of the $\tilde{A}^2A_1$-$\tilde{X}^2B_1(0_0^0)$ band of PH_2 was later reported, in which the observed perturbations for the upper state were also briefly discussed [18]. Recently, a dispersed fluorescence study together with *ab initio* calculations for the $\tilde{X}^2B_1$ and $\tilde{A}^2A_1$ states of PH_2 was performed by Jakubek *et al.* [19].

The PH_2 radical can be attributed to a bent asymmetric top of C_{2v} symmetry in both ground and excited states, with three vibrational modes labeled v_1 (A_1, As–H symmetric stretch), v_2 (A_1, bent), and v_3 (b_2, As–H asymmetric stretch), respectively. The bond angle of the $\tilde{A}^2A_1$ state is determined to be about 123.20°, much larger than 91.70° in the ground state [17]. Similar to those of the NH_2 radical, the two lowest electronic states of PH_2, $\tilde{X}^2B_1$ and $\tilde{A}^2A_1$, correlate with the $^2\Pi$ state in the limit of a linear configuration that is split by a Renner-Teller interaction. This may make the electronically excited states of PH_2 be perturbed extensively by the high-lying vibrational levels of its ground state. In Refs.[7, 18], numerous rotational perturbations in the $\tilde{A}^2A_1(0^0)$ state were reported and briefly discussed.

However, precise molecular constants and perturbations for the excited vibronic states have not yet been determined. In this work we present a cavity ringdown spectroscopy (CRDS) study on the absorption spectra of PH_2 with high sensitivity and high resolution, in an attempt to reveal the rotational perturbations in the excited vibronic states (v_2'>0).

CRDS [20] is an absorption-based technique capable of achieving ultrahigh sensitivity and high resolution. It measures the loss rate of light out of an optical cavity

[†]Current address: Institute for Lasers, Life and Biophotonics Amsterdam, De Boelelaan 1081, NL 1081 HV Amsterdam, the Netherlands.
[*]Author to whom correspondence should be addressed. E-mail: yangchen@ustc.edu.cn

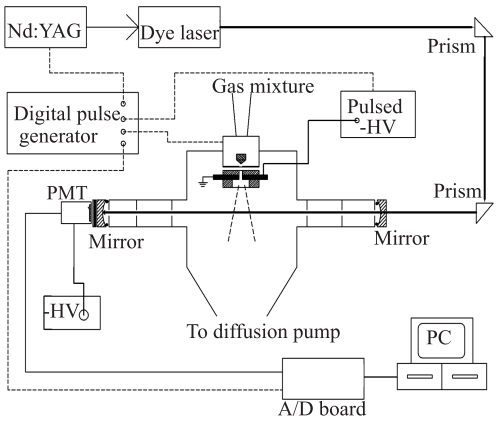

FIG. 1 Schematic diagram of the pulsed discharge and the cavity ringdown spectroscopy apparatus.

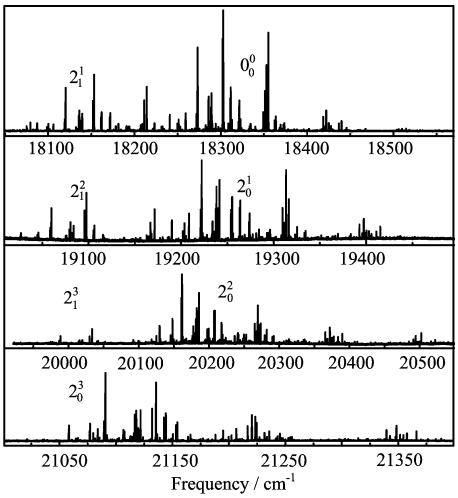

FIG. 2 CRDS spectra of the observed bands of PH_2 in 465–555 nm. Seven vibronic bands was assigned to two progressions of 0_0^0, 2_0^n, and 2_1^n (n=1–3).

formed by two highly reflective mirrors, which can be characterized with a ringdown signal that has a decay profile expressed as

$$I(t) = I_0 \mathrm{e}^{-t/\tau} \tag{1}$$

$$\tau = \frac{L}{c(1-R+\alpha l)} \tag{2}$$

$$\tau_0 = \frac{L}{c(1-R)} \tag{3}$$

where τ and τ_0 are the ringdown times of the cavity with the absorption sample present and absent, respectively, L is the optical length of the cavity, c is the speed of light, R is the averaged reflectivity of the two cavity mirrors, α and l are the absorption coefficient and the length of the sample, respectively.

II. EXPERIMENTS

A schematic of the supersonic jet apparatus and the cavity ringdown spectrometer is shown in Fig.1. The PH_2 radicals were produced by DC discharge of a jet-cooled beam of the PH_3 molecules. A gas mixture of 2%PH_3 (99.999%, Nanjing) and 0.5%SF_6 (99.99%, Nanjing) seeded in argon at a stagnation pressure of ∼600 kPa passed through a pulsed nozzle (General Valve, Series 9) of 0.5 mm orifice diameter operating with a pulse duration of 150 μs into the vacuum chamber. A pair of aluminum round bars with flat head (located at ∼2 mm downstream from the nozzle) used for discharge was set with a spacing of ∼1.5 mm, and was supplied with a synchronized pulsed high voltage (−1200 V, ∼200 μs). The gas beam was intersected perpendicularly with a laser beam ∼25 mm downstream from the electrodes. The background pressure was about 2 and 20 mPa, with and without operation of the gas beam, respectively.

The setup is operated at 10 Hz, which was determined by the maximum repetition rate of a tripled Nd:YAG laser (Spectra physics, GCR-170) that was used to pump a dye laser system (Sirah, PrecisionScan). This commercial laser system is standard configured with a double grating (1800 line/mm) resonator and has a typical best bandwidth in this wavelength range of ∼0.07 cm^{-1}, when operated as described in the manual. A relatively simple trick was allowed to substantially improve the achievable laser resolution. The 2nd order diffraction of the Littrow grating was used instead of the first order, yielding a laser bandwidth improvement with a factor of 2. Absolute laser wavelength was calibrated by a wavemeter (Coherent, WaveMaster 33-2650) with a resolution of 0.016 cm^{-1}.

Cavity ringdown was achieved by injecting a small fraction of the laser pulse into a high-finesse optical cavity (85-cm long) constituted by two dielectrically coated plano-concave mirrors (Los Gatos Research, R@500 nm>99.99%; Layertec, R@550 nm>99.98%) with a curvature radius of 1 m. The mirrors were held in adjustable mirror mounts attached to the two ends of the chamber with flexible bellows and fat O-rings. The injected laser beam was reflected many times between the mirrors, and the light that leaked out of the cavity first passed through a narrow bandpass filter and a diffuser plate, and was then detected by a photomultiplier tube (PMT, Hamamasu, R1428). The PMT signal was digitized by an A/D board (Gage, CS14200, 200 MHz, 14 bit) and then transferred to a personal computer. The data were analyzed in real time by a LabVIEW program, which was developed for processing the digital signal and extracting the ringdown times.

III. RESULTS AND DISCUSSION

By scanning the dye laser with a step of 0.5 pm/s, the absorption spectra of PH_2 were obtained in the laser wavelength range of 465–555 nm. In Fig.2, the observed

DOI:10.1088/1674-0068/24/01/8-15

TABLE I Molecular parameters (state origin T_v, rotational constant A, B, C, and Δ_K, Δ_{JK}, Δ_J for K^4, $J(J+1)K^2$, $J^2(J+1)^2$ quartic centrifugal distortion respectively, and ε_{aa}, ε_{bb}, ε_{cc} for aa, bb, cc spin-rotation parameter, respectively, and quartic spin rotation parameter Δ^s_N, Δ^s_{NK}, Δ^s_{KN}, Δ^s_K, all in cm^{-1}) for PH_2.

Parameter	$\tilde{X}^2B_1(2_1)$	$\tilde{A}^2A_1(0^0)$	$\tilde{A}^2A_1(2^1)$	$\tilde{A}^2A_1(2^2, K_a\leq3)$
T_v	1101.8590(41)[a]	18276.5672(25)	19225.6773(33)	20165.4040(45)
A	9.4488(11)	20.39375(46)	23.50585(55)	28.03713(96)
B	8.25545(91)	5.60836(34)	5.64489(44)	5.73422(72)
C	4.15792(56)	4.29805(39)	4.25421(50)	4.16329(81)
Δ[b]	0.01354	0.00532	0.01537	0.03014
Δ_K	$5.10(12)\times10^{-3}$	0.032446(38)	0.063147(45)	0.15123(12)
Δ_{JK}	$-2.276(67)\times10^{-3}$	$-1.342(23)\times10^{-3}$	$-3.082(25)\times10^{-3}$	–0.010552(53)
Δ_J	$2.61(15)\times10^{-4}$	$2.411(58)\times10^{-4}$	$4.24(72)\times10^{-5}$	$6.99(14)\times10^{-4}$
δ_K	$-1.2(10)\times10^{-4}$	$9.1(23)\times10^{-4}$	1.258×10^{-4}	0.03144(57)
Δ'_J	$5(15)\times10^{-6}$	$3.8(11)\times10^{-5}$	$3.3(17)\times10^{-5}$	$2.01(31)\times10^{-4}$
ε_{aa}	−0.3038(69)	1.2207(37)	1.7582(49)	2.8809(82)
ε_{bb}	−0.0784(73)	0.0151(31)	0.0225(39)	0.0161(56)
ε_{cc}	−0.0580(49)	–0.0520(34)	–0.0368(43)	–0.0323(62)[c]
Δ^s_N	$5.52(15)\times10^{-3}$	$-1.3(61)\times10^{-5}$[c]	$-1.067(76)\times10^{-3}$	$-4.42(14)\times10^{-3}$
Δ^s_{NK}	-0.17448(46)	0.03395(22)	0.08998(28)	0.16100(62)
Δ^s_{KN}	0.17454(59)	–0.02776(21)	-0.05650(24)	–0.08662(47)
Δ^s_K	$2.57(91)\times10^{-3}$	–0.01361(34)	–0.05349(45)	–0.13766(97)
Lines	123	186	180	171
σ	0.054	0.034	0.044	0.059

[a] The numbers in parentheses are the 1σ error limits.
[b] $\Delta=I_C-I_B-I_A$, in amu Å^2.
[c] Fixed.

seven bands with fine rotational structures were shown. The spectral profiles of all these bands with recognizable branch structures are very similar to each other. Based on some previous studies [7, 17], the spectra shown in Fig.2 can be readily assigned as the 0^0_0, 2^n_0, and 2^n_1 (n=1–3) bands for the $\tilde{A}^2A_1$-$\tilde{X}^2B_1$ transition. Using the molecular parameters and term values reported in Refs.[7, 17], rotational assignments for the 0^0_0 and 2^n_0 (n=1–3) bands can be given. Since all the bands observed in this work have very similar rotational structures, the preliminary assignments for the 2^n_1 (n=1–3) bands can also be obtained and checked using the term values for the excited vibronic states.

Once the rotational assignments of all the bands were obtained, we fitted the data to obtain a set of molecular constants by the least-squares analysis, and then checked the assignments using the fitted results. The observed rotational lines were fitted using an effective Hamiltonian [21, 22]:

$$H_{\rm eff} = H_{\rm rot} + H_{\rm cd} + H_{\rm sr} \quad (4)$$

where $H_{\rm rot}$ is the rotational Hamiltonian, $H_{\rm cd}$ the centrifugal distortion effect term, and $H_{\rm sr}$ the spin-rotation interaction term. When fitting the 0^0_0 and 2^n_0 (n=1–3) bands, we varied the excited-state constants and the band origins with the parameters for the 0_0 state taken from Ref.[16] fixed. The parameters for the 2_1 state were obtained by fitting the 2^1_1 band with the parameters of the 2^1 state fixed. The least-squares fit was accomplished by the PGOPHER program [23]. In present work, all the five observed bands were fully rotationally analyzed, yielding the precisely determined molecular constants and the rotational term values of the 2_1 state and the excited vibronic states.

A. The 0^0_0, 2^1_1, and 2^1_0 bands

By using the Hamiltonian described by Eq.(4), all observed rotational lines for the 0^0_0, 2^1_1, and 2^1_0 bands were fitted, with reasonably small standard deviations of 0.034, 0.054, and 0.044 cm^{-1}, respectively. As an example, the simulated spectra for the 0^0_0 and 2^1_1 bands were displayed in Fig.3, which match nicely with the observed spectrum shown in Fig.3. The obtained molecular parameters are listed in Table I, while the observed rotational term values as well as the differences between the observed and calculated (o–c) term values are listed in Table II. Our results are in reasonably good agreement with those of previous studies. The obtained molecular parameters for the 2^1 state have higher precision than those given in Refs.[7, 17], which enabled us to derive the rotational term values.

DOI:10.1088/1674-0068/24/01/8-15

TABLE II Rotational term values and the o–c deviations (in cm^{-1}) of PH_2.

State			$\tilde{X}^2B_1(2_1)$		$\tilde{A}^2A_1(0^0)$		$\tilde{A}^2A_1(2^1)$		$\tilde{A}^2A_1(2^2)$		$\tilde{A}^2A_1(2^3)$	
T_v			1101.861		18276.569		19225.677		20165.399		21094.1330	
	$N_{Ka,Kc}$	J	Obs.	o–c/10^{-3}	Obs.	o–c/10^{-3}	Obs.	o–c/10^{-3}	Obs.	o–c/10^{-3a}	Obs.	o–c/10^{-3a}
$N_{0,N}$	1_{01}	1.5	12.374	–10	9.899	3	9.868	–26	9.923	45	9.879	3
		0.5	12.488	18	9.919	–5	9.890	–18	9.912	0	9.882	–2
	2_{02}	2.5	34.022	–12	29.602	–7	29.586	–18	29.486	–71	29.569	1
		1.5	34.201	21	29.647	–9	29.664	27	29.648	5	29.569	–1
	3_{03}	3.5	63.725	–4	58.962	–2	58.975	7	58.911	21	58.930	–12
		2.5	63.874	6	59.019	–13	58.991	–44	59.068	3	58.921	4
	4_{04}	4.5	101.662	6	97.701	–12	97.758	1	97.691	16	97.772	–26
		3.5	101.762	–29	97.804	2						
	5_{05}	5.5			145.564	1	145.681	–24	145.645	–23	145.891	26
		4.5			145.629	–40	145.873	–15	146.273	0	145.699	1
	6_{06}	5.5			202.305	–20						
$N_{1,N}$	1_{11}	1.5	13.516	1	24.953	15	28.091	–7	32.773	–45	39.960	27
		0.5	13.801	26	24.077	–3	26.815	–23	30.704	1	36.473	–39
	2_{12}	2.5	34.248	–4	43.301	–27	46.351	–22	50.972	61	57.669	6
		1.5	34.467	19	42.957	32	45.728	–8	49.941	–21	56.388	4
	3_{13}	3.5	63.805	49	70.954	–4	73.894	26	78.159	–75	84.220	–71
		2.5	63.880	–26	70.764	24	73.511	30	77.721	–54	83.864	58
	4_{14}	4.5	101.661	3	107.812	84	110.489	6	114.688	28		
		3.5	101.815	39	107.600	–26	110.292	11	114.657	30		
	5_{15}	5.5	147.855	–13	153.546	2					162.020	24
		4.5	148.169	11								
$N_{1,N-1}$	1_{10}	1.5	17.563	–41	26.257	–1	29.525	32	34.229	–5	41.411	–41
		0.5	17.864	–18	25.338	–14	28.205	7	32.134	4	37.898	45
	2_{11}	2.5	46.570	62	47.290	16	50.523	–29	55.270	78	62.376	7
		1.5	46.765	12	46.790	1	49.866	17	54.221	0	60.738	7
	3_{12}	3.5	86.053	–12	78.816	–11	82.211	2	86.726	–49	94.047	24
		2.5	86.420	–10	78.483	–11	81.747	15	86.309	18	93.109	–16
	4_{13}	4.5	133.334	7	120.781	–16	124.315	–27	128.806	–4		
		3.5	134.156	10	120.549	1	124.019	–11	128.704	–55	136.070	12
	5_{14}	5.5			173.033	–16	176.807	–20	181.218	72	188.338	–14
		4.5			172.861	2	176.635	–54	181.631	24	189.657	–14
$N_{2,N-1}$	2_{21}	2.5	49.937	16	91.730	–9	104.005	–23	121.304	6	146.373	–19
		1.5	50.453	1	89.810	18	101.295	42	117.081	–7	139.790	–38
	3_{22}	3.5	87.034	–46	121.267	8	133.635	104	150.816	2	175.776	–25
		2.5	87.669	25	119.980	26	131.650	48	148.090	57	171.669	–224
	4_{23}	4.5	133.489	–10	160.684	1	173.026	42	190.182	–37	214.672	–2
		3.5	134.374	–31	159.717	9	171.395	–115	188.379	24	212.654	–3
	5_{24}	5.5	187.998	13	209.866	–52	222.282	–13	239.281	10		
		4.5	189.995	34			221.182	45	238.241	–51		
	6_{25}	6.5					281.404	–57				
		5.5			268.182	29	280.564	84				
$N_{2,N-2}$	2_{20}	2.5	53.060	–38	91.840	19	104.093	–12	121.317	–30	146.412	20
		1.5	53.535	–21	89.872	–3	101.302	–30	117.154	10	139.866	38
	3_{21}	3.5	97.896	19	121.728	60	133.901	–10	151.087	16	176.021	221
		2.5	98.235	–4	120.398	35	132.060	67	148.264	–44	171.893	5
	4_{22}	4.5	154.953	–12	161.885	–4	174.110	5	191.010	34	214.679	6
		3.5	155.411	2	160.889	–29	172.718	51	189.136	–31	212.828	172

To be continued.

DOI:10.1088/1674-0068/24/01/8-15

Table II continued.

State			$\tilde{X}^2B_1(2_1)$		$\tilde{A}^2A_1(0^0)$		$\tilde{A}^2A_1(2^1)$		$\tilde{A}^2A_1(2^2)$		$\tilde{A}^2A_1(2^3)$	
T_v			1101.861		18276.569		19225.677		20165.399		21094.1330	
	N_{K_a,K_c}	J	Obs.	o–c/10^{-3}	Obs.	o–c/10^{-3}	Obs.	o–c/10^{-3}	Obs.	o–c/10^{-3a}	Obs.	o–c/10^{-3a}
$N_{2,N-2}$	5_{23}	5.5			212.651	18	224.911	85			262.026	–208
		4.5			211.910	32	223.836	60	240.165	19	262.401	–21
$N_{3,N-2}$	3_{31}	3.5	104.652	32	197.158	–16	219.130	–43	258.247	–30	306.146	146
		2.5	105.363	1	194.192	6	262.901	–39	252.339	12	297.672	22
	4_{32}	4.5			236.674	–41	259.661	–36	297.800	–35	345.995	113
		3.5			234.448	–27	312.673	39	293.429	36	339.526	–46
	5_{33}	5.5	220.865	1	286.298	–11	310.127	73	347.207	–57		
		4.5			284.540	6	219.130	–43	344.353	0		
	6_{34}	5.5			344.454	–13						
$N_{3,N-3}$	3_{30}	3.5	106.701	–83	197.164	–14	223.320	–10	258.306	26	305.934	–66
		2.5	107.416	–2	194.185	–4	219.167	–9	252.333	1	297.632	–18
	4_{31}	4.5	166.601	–7	236.712	–26	262.973	14	297.911	54	345.821	–61
		3.5			234.424	–75	259.654	–63	293.384	–36	399.674	101
	5_{32}	5.5			286.415	16	312.705	–3	347.367	18		
		4.5			284.645	19	310.090	–45	344.450	–8		
$N_{4,N-3}$	4_{41}	4.5			339.917	29	382.990	79	438.715	9		
		3.5			335.977	18	377.725	52	431.489	–6		
	5_{42}	5.5					432.701	24	488.324	–7		
		4.5							482.540	–44		
$N_{4,N-4}$	4_{40}	4.5	178.790	–7	339.887	–1	382.945	34	438.727	20		
		3.5			335.959	1	377.714	41	431.486	–10		
	5_{41}	5.5					432.600	–78	488.329	–1		
		4.5			386.280	35	428.295	10	500.562	40		

[a] The band origin shift for each K'_a>1 level has been deducted in the o–c deviations.

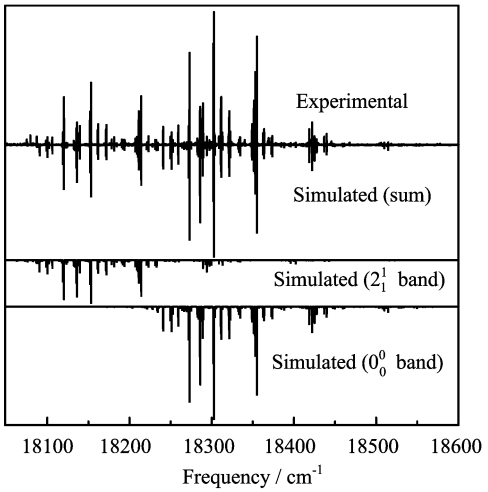

FIG. 3 Rotationally resolved spectra of the 0_0^0 and 2_1^1 bands of PH_2. The upper trace is the experimental spectrum, while the lower three traces are the simulated spectra for the 0_0^0, 2_1^1 bands, and their sum, respectively.

In our spectra, only the levels with K'_a≤4 in the upper states were observed, and most of the |o−c| deviations are quite small, as shown in Table II. Hirota *et al.* pointed out that the rotational levels, 2_{12} (F_1), 5_{24} (F_1), and 4_{31} (F_1, F_2), of the 0^0 state may be perturbed [18], but the |o−c| deviations for these levels we obtained do not show any large shifts. The perturbations in the K'_a≤4 levels of the 0^0 and 2^1 states are expected to be very small.

B. The 2_0^2 band

For 2_0^2 band, the Hamiltonian described by Eq.(4) still gave us a reasonably good fit for the K'_a≤3 levels, with a little bit larger standard deviation of 0.059 cm^{-1}. The obtained molecule parameters are also listed in Table I. However, we found that all the rotational lines with K'_a=4 are of rather large |o–c| deviations (up to ∼3 cm^{-1}), which implies that there may exist large perturbations in the K'_a=4 level. And we also found that the rotational term values with K'_a=4 can be fitted by using the same Hamiltonian in which the rotational constant A is fixed. To reveal the perturbations in all the observed rotational levels, we refitted the term values of K'_a= 0, 1, 2, 3, and 4 levels in the upper state, respectively, the results are listed in Tables II and III.

DOI:10.1088/1674-0068/24/01/8-15

TABLE III Molecular parameters (in cm^{-1}) for each K_a level in the 2^2 and 2^3 states of PH_2.

Parameter	2^2				2^3		
	K_a=0,1	K_a=2	K_a=3	K_a=4	K_a=0,1	K_a=2	K_a=3
T_v	20165.3894(46)[a]	20165.0705(55)	20164.8346(58)	20167.5946(51)	21094.0765(28)	21092.2031(52)	21088.392(17)
$\Delta(T_v)$[b]	0	–0.3189	–0.5548	3.3121	0	–1.8734	–5.6845
A	28.1034(56)	28.1034	28.1034	28.1034	35.1401(37)	35.1401	35.1401
B	5.72965(72)				5.82685(41)		
C	4.15943(79)				4.06362(38)		
$(B+C)/2$	4.94454	4.95817(60)	4.92732(53)	4.91030(50)	4.94524	5.00973(54)	4.9838(25)
$\Delta_K\times10^3$	157.7(55)	158.20(34)	150.929(72)	152.518(20)	291.9(37)	314.96(32)	314.96
$\Delta_{JK}\times10^3$	–8.43(46)	–14.877(90)	–10.226(34)	–12.316(13)	–19.32(27)	–37.10(10)	–37.10
$\Delta_J\times10^3$	0.544(19)	1.220(16)	0.622(13)	1.2821(74)	2.8524(70)	5.515(22)	5.515
$\delta_K\times10^3$	31.02(46)				65.13(30)		
$\delta_J\times10^3$	0.221(24)				–3.0786(95)		
ε_{aa}	2.96330	2.8540(99)	2.8794(59)	3.0740(37)	5.207(20)	4.4997(93)	3.857(16)
$\varepsilon_{bb}\times10^3$	3.71(28)	28.1(69)	18.8(84)	11.5(85)	178.5(32)	457.7(78)	1257(33)
$\varepsilon_{cc}\times10^3$	–33.5(60)	–36.6(76)	–30.7(93)	–71.5(85)	–196.0(36)	–221.3(78)	–202(33)
$\Delta^s_N\times10^3$	–3.42(18)	–4.91(16)	–7.97(13)	–7.952(82)	1.297(83)	2.16(22)	2.16
$\Delta^s_{NK}\times10^3$	141.4(57)	163.7(10)	165.00(40)	165.16(16)	351.6(18)	356.8(12)	356.8
$\Delta^s_{KN}\times10^3$	–104(35)	–840(73)	–759(31)	–75.90(13)	–194.9(25)	–198.82(80)	–198.82
$\Delta^s_K\times10^3$	–25(30)	–146.5(25)	–152.00(66)	–151.61(23)	–239(20)	–249.0(23)	–249.0
Lines	87	46	38	27[c]	82	37	20
σ	0.043	0.039	0.035	0.026	0.025	0.031	0.073

[a] The numbers in parentheses are the 1σ error limits.
[b] $\Delta(T_v)= T_v(K_a)–T_v(K_a=0 \text{ and } 1)$.
[c] Another 11 lines observed in this level were not contained in the least-squares fit.

The standard |o−c| deviations and the deviations are all reasonably improved.

As shown in Tables I and III, the obtained parameters for K'_a=0, 1, 2, 3, and 4 levels are almost equal to those obtained by fitting the K'_a=0–3 levels altogether, and almost all the new |o−c| deviations are reasonably small. But apparent changes appear in the band origins obtained by fitting the K'_a=2, 3, and 4 levels, especially in the K'_a=4 level (3.3 cm^{-1}). We suggest that the perturbations in the 2^2 state may mainly be dependent on the K'_a values, quite small for the levels with K'_a=0 and 1, while larger for the K'_a=2, 3, and 4 levels (–0.3189, –0.5548, and 3.3121 cm^{-1}, respectively).

C. The 2^3_0 band

Special care was taken in the analysis of the 2^3 state. The rotational lines of the 2^3_0 band could not be satisfactorily fitted by the Hamiltonian given in Eq.(4). When all the observed 139 lines with $K'_a\leq3$ in upper states in our spectra were used for the fit, the standard deviations were found to be very large ($\sim$0.098 cm^{-1}) and the obtained rotational constants were not entirely reasonable. The fitting routine including all the observed transitions yields the values of constants B' and C' as 5.7934 and 4.1583 cm^{-1}, respectively, which depart considerably from those obtained from the lower vibronic states (0^0, 2^1, and 2^2). Such a large discrepancy was also found by Berthou *et al.* [7], who proposed that this may be due to the perturbations in the K'_a>0 levels or a breakdown of the Hamiltonian. In order to obtain the precise molecular constants and rotational term values of the 2^3 state, we fitted the term values for the K'_a=0, 1, 2, and 3 levels in the upper state, respectively, as what we have done for the 2^2_0 band. The fitted results are listed in Tables II and III.

In our results, the standard deviations and the |o−c| deviations are quite small for the K'_a=0, 1 and 2 levels, but still very large for the K'_a=3 level, as shown in Tables II and III. Again, there appear very large changes in the band origins and the spin-rotation interaction constants for both K'_a=2 and 3 levels. The band origin for K'_a=0 and 1 levels lies very close to the value derived from the lower vibronic states, which might indicates the perturbations in the K'_a=0 and 1 levels should be very small. While for the K'_a=2 level, the perturbations lead to a shift of –1.8734 cm^{-1} in the band origin. Note that a few rotational levels, *i.e.*, 3_{21} (F_1), 3_{22} (F_2), 4_{22} (F_2), and 5_{23} (F_1), with K'_a=2 related to 11 observed lines also show large |o−c| deviations. The perturbations in the K'_a=3 are much more complicated

DOI:10.1088/1674-0068/24/01/8-15

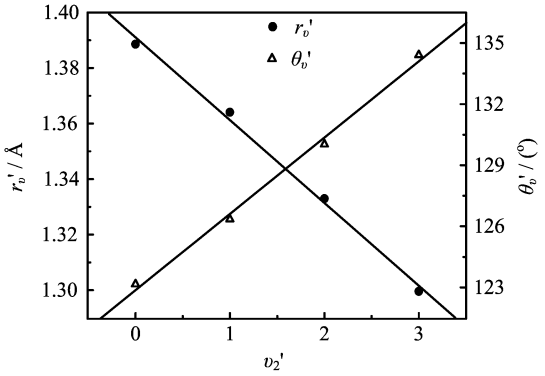

FIG. 4 The structural parameters (r'_v and θ'_v) *vs.* v'_2 of the $\tilde{A}^2A_1$ state of PH_2.

TABLE IV The structural parameters of PH_2.

State	$\theta_v/(^\circ)$	r_v/Å
$\tilde{X}^2B_1(0_0)$[a]	91.69(1)	1.4178(1)
$\tilde{X}^2B_1(2_1)$	92.09(1)	1.3985(2)
$\tilde{A}^2A_1(0^0)$	123.16(1)	1.3886(1)
$\tilde{A}^2A_1(2^1)$	126.34(1)	1.3641(1)
$\tilde{A}^2A_1(2^2)$	130.03(2)	1.3330(2)
$\tilde{A}^2A_1(2^3)$	134.41(3)	1.2996(4)

[a] Calculated using the parameters from Ref.[16].

than those in the lower K'_a level, because not only a shift of about –5.68 cm^{-1} in the band origin was found but also most of the rotational lines showed large |o−c| deviations of about 0.1 cm^{-1}.

After the rotational analysis and fittings for the 0^0_0, 2^1_1, and 2^n_0 (n=1–3) bands have been completed, the effective molecular structures of PH_2 for each vibronic state can be calculated using the rotational constants listed in Table I, giving the results that are summarized in Table IV. Figure 4 shows a plot of the structural parameters, r'_v and θ'_v, for the excited state *vs.* the vibrational quantum number v'_2, from which a reasonably good linear relationship can be seen. We can thus derive the equilibrium structures as follows: For the $\tilde{X}^2B_1$ state, r''_e=1.4275 Å, θ''_e=91.49°. For the $\tilde{A}^2A_1$ state, r'_e=1.4059(32) Å, θ'_e=120.99(43)°.

An approximate formula for the inertial defect derived by Oka *et al.* can be used to check our results [24]. The expression for the inertial defect of C_{2v} triatomic molecules can be written as

$$\Delta = \sum_s \Delta_s \left(v_s + \frac{1}{2} \right) \tag{5}$$

where s is the vibration mode, v_s the vibrational number, and Δ_s the contribution of each vibration mode to the inertial defect. In our spectra, both the v_1 and v_3 modes are not excited, thus we have

$$\Delta = \Delta_2 \left(v_2 + \frac{1}{2} \right) + \frac{1}{2} (\Delta_1 + \Delta_3) \tag{6}$$

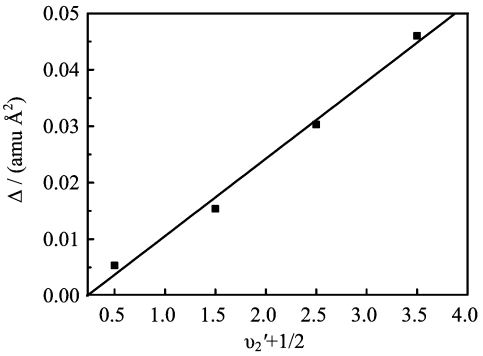

FIG. 5 The observed inertial defect Δ *vs.* $(v'_2 + 1/2)$ of the state $\tilde{A}^2A_1$ of PH_2.

Figure 5 shows the plot of Δ *vs.* the quantum number $(v'_2+1/2)$, which exhibits a good linearity. This in turn indicates that the inertial defect values we obtained are reasonable.

In our spectra, large perturbations have been found in the excited vibronic states. Similar behaviors have also been found in other molecules, such as H_2O [25], SiH_2 [26], and AsH_2 [27]. According to study of Berthou *et al.* [7], the perturbations in the 0^0 states of PH_2 may most probably come from the high-lying vibrational levels of the ground state, as there are no any other electronic states below the $\tilde{A}^2A_1$ state. The lowest quartet state which has not yet been observed may be another possible perturber, but energetically it should lie higher than the $\tilde{A}^2A_1$ state. Most of the perturbations we observed should therefore be caused by the same reason as proposed by Berthou *et al.* [7]. Nonetheless, from the above analysis, we can claim that the rotational levels with large perturbations in the K'_a=2 and 3 levels of the 2^3 states may originate not only from the high-lying vibrational levels of the ground state, but also from the lowest quartet state, $^4A_2$, which may be dissotiative and correlated with $P(^4S_u)+H_2(^1\Sigma^+_g)$ at 16384 cm^{-1} [28].

IV. CONCLUSION

We have reported the cavity ringdown spectra of jet-cooled PH_2 radicals recorded in the wavelength range of 465–555 nm. Seven vibronic bands with fine rotational structures were observed and assigned as the 0^0_0, 2^n_0, and 2^n_1 (n=1–3) bands of the $\tilde{A}^2A_1$-$\tilde{X}^2B_1$ electronic transition. The spectroscopic constants for these bands were improved with reasonably high precision. Perturbations observed in the excited vibronic states were also discussed.

DOI:10.1088/1674-0068/24/01/8-15

V. ACKNOWLEDGMENTS

This work was supported by the National Natural Science Foundation of China (No.20673107), the National Key Basic Research Special Foundation of China (No.2007CB815203), and the Chinese Academy of Sciences (No.KJCX2-SW-H08).

[1] D. A. Ramsay, Nature **178**, 374 (1956).
[2] H. Guenebaut and B. Pascat, J. Chim. Phys. **61**, 592 (1964).
[3] H. Guenebaut, B. Pascat, and J. M. Berthou, J. Chim. Phys. **62**, 867 (1965).
[4] R. N. Dixon, G. Duxbury, and D. A. Ramsay, Proc. R. Soc. London Ser. A **296**, 137 (1967).
[5] B. Pascat, J. M. Berthou, H. Guenebaut, and D. A. Ramsay, C. R. Acad. Sci. Paris Ser. B **263**, 1397 (1966).
[6] B. Pascat, J. M. Berthou, J. C. Prudhomme, H. Guenebaut, and D. A. Ramsay, J. Chim. Phys. **65**, 2022 (1968).
[7] J. M. Berthou, B. Pascat, H. Guenebaut, and D. A. Ramsay, Can. J. Phys. **50**, 2265 (1972).
[8] R. E. Huie, N. J. T. Long, and B. A. Thrush, J. Chem. Soc. Faraday Trans. II **74**, 1253 (1978).
[9] P. B. Davies, D. K. Russel, and B. A. Thrush, Chem. Phys. Lett. **37**, 43 (1976).
[10] P. B. Davies, D. K. Russel, B. A. Thrush, and H. E. Radford, Chem. Phys. **44**, 421 (1979).
[11] G. W. Hills and A. R. W. McKeller, J. Chem. Phys. **71**, 1141 (1979).
[12] A. R. W. McKeller, Discuss. Faraday Soc. **71**, 63 (1981).
[13] R. F. Curl, Y. Endo, M. Kakimoto, S. Saito, and E. Hirota, Chem. Phys. Lett. **53**, 536 (1978).
[14] M. Kakimoto and E. Hirota, J. Mol. Spectrosc. **94**, 173 (1982).
[15] Y. Endo, S. Saito, and E. Hirota, J. Mol. Spectrosc. **97**, 204 (1983).
[16] M. Kajita, Y. Endo, and E. Hirota, J. Mol. Spectrosc. **124**, 66 (1987).
[17] Y. Chen, Q. Zhang, D. Zhang, C. Chen, S. Yu, and X. Ma, Chem. Phys. Lett. **223**, 104 (1994).
[18] E. Hirota and M. Kakimoto, J. Mol. Struct. **352/353**, 379 (1995).
[19] Z. J. Jakubek, P. R. Bunker, M. Zachwieja, S. G. Nakhate, and B. Simard, J. Chem. Phys. **124**, 094306 (2006).
[20] J. J. Scherer, J. B. Paul, A. O'Keefe, and R. J. Saykally, Chem. Rev. **97**, 25 (1997).
[21] T. J. Sears, Comput. Phys. Rep. **2**, 1 (1984).
[22] T. J. Sears, Comput. Phys. Commun. **34**, 123 (1984).
[23] C. M. Western, *PGOPHER, a Program for Simulating Rotational Structure*, University of Bristol, http://pgopher.chm.bris.ac.uk.
[24] T. Oka, and Y. Morino, J. Mol. Spectrosc. **8**, 9 (1962).
[25] J. W. C. Johns, Can. J. Phys. **45**, 2639 (1967) .
[26] I. Dubois, Can. J. Phys. **46**, 2485 (1967).
[27] R. N. Dixon, G. Duxbury, and H. M. Lamberton, Proc. R. Soc. London Ser. A **305**, 271 (1968).
[28] *JANAF Thermochemical Tables*, Washington: U. S. National Bureau of Standards, (1971).

DOI:10.1088/1674-0068/24/01/8-15